MADRID
inter.noise 2019
June 16 - 19
NOISE CONTROL FOR A BETTER ENVIRONMENT

Numerical Analysis of the Instabilities Behind a Blunt Slat Trailing-Edge

Botero-Bolívar, Laura[1]
Acevedo-Giraldo, Daniel
Pereira, Lourenço T.
Catalano, Fernando M.
University of São Paulo
Av. Trab. São Carlense, 400, São Carlos - SP, Brazil

Reis, Danillo C.[2]
Coelho, Eduardo L. C.
EMBRAER
Av. Brigadeiro Faria Lima 2170, São José dos Campos - SP, Brazil

ABSTRACT

Concerns about the noise generated by the structure of aircraft have significantly increased over the past years due to reductions in the engine noise and tighter regulations established by certifying entities. Slat is one of the most important sources of airframe noise, since it generates a noise spectrum composed of mid-frequency tones, a broadband component, and a high-frequency hump. This article addresses a detailed analysis of the high-frequency tone generation and its relation to the slat trailing-edge thickness. Numerical simulations of a typical three-element airfoil were conducted by PowerFLOW 5.3 software at 1 million Reynolds number and the noise was propagated according to the Ffowcs William-Hawking methodology. The high spatial and temporal resolution in the simulations aimed to capture variations in the slat trailing-edge thickness. The results showed the presence of a strong vortex shedding behind the slat, which is highly related to the high-frequency tone and the blunt slat trailing-edge. The frequency of the tone in the far-field spectrum is in agreement with that in the vortex shedding. The Strouhal number calculated with the use of the boundary layer displacement thickness as the characteristic length was constant for all cases and close to 0.4.

Keywords: Airframe Noise, Slat Noise, Vortex Shedding, Computational Aeroacoustics, Slat Trailing-Edge
I-INCE Classification of Subject Number: 21
http://i-ince.org/files/data/classification.pdf

[1] laura.boterobol@usp.br
[2] danillo.reis@embraer.com.br

1. INTRODUCTION

Since the 1960's, aircraft noise has become one of the most important topics in aeronautic sciences due to increases in both air traffic and population close to main worldwide airports. As a consequence, tighter regulations, several programs and researches have been developed in different aeronautic institutions towards reductions in the aircraft noise [1, 2]. Aircraft noise is composed of engine noise and airframe noise; the former refers to the noise generated by the components of the aircraft propulsion system, whereas airframe noise is generated by the fluid-structure interaction [3, 4]. When aircraft noise first came to the forefront, engines were the main source and the focus of noise reduction. However, over the past few decades, they have become significantly quieter due to the incorporation of the high-by-pass technology [4, 5], and engine noise is currently the major contribution to the overall aircraft noise during take-off, when the maximum power is required. On the other hand, airframe noise is the most significant component in the landing approach stage [6].

The main sources of airframe noise are landing gear and high-lift systems (slats and flaps) and their rank highly depends on the geometry and operational conditions of each aircraft. According to Dobrzynski, W. et al., (2015) [2], a wing in the high-lift configuration is 10 dB noisier than a wing in the cruise configuration. The slat noise is generated by the complex flow formed in the gap between the slat and the wing main element and the unsteady loads caused by the interaction of such flow with the downstream elements, i. e., slat upper surface and trailing-edge and wing main element leading edge (Figure 1a) [5, 7]. Such a phenomenon causes a typical slat spectrum (Figure 1b) composed of mid-frequency tones, a broadband component that decrease in function of the frequency, and a high-frequency hump. The mid-frequency tones are attributed to a feedback loop created between the vortices detached from the slat cusp and acoustic waves generated in the reattachment point [10]. The broadband noise is probably caused by the interaction of the shear-layer and the wing components [11]. Finally, the high-frequency hump is related to the vortex shedding behind blunt slat trailing-edges [12]. Such vortices are governed by Karman vortex, which became a dipole of a specific frequency, represented by a single tone at high frequency.

This paper reports on an analysis of the high-frequency hump and its relation to the vortex shedding and the slat trailing-edge thickness. Simulations were performed with varied slat trailing-edge thicknesses of a conventional mid-range aircraft three-element airfoil (slat, main wing element, and flap). The numerical analyses were conducted at 1.1 x 10^6 Reynolds number and 0.101 Mach number on PowerFLOW software, which uses the Lattice Boltzmann Method (LBM) as a fluid solver, and the Ffocws William-Hawking (FW-H) acoustic analogy for resolving the acoustic far-field.

2. NUMERICAL METHODOLOGY

Numerical simulations were performed on PowerFLOW 5.3® commercial software, which focuses on aeroacoustic simulations and uses LBM for resolving the flow properties. The method is based on the resolution of the Lattice-Boltzmann equation in discrete cells with appropriate symmetries, which is essentially the kinetic equation that resulted from the ensemble-averaging of the discrete dynamics of the Frish-Hasslacher-Pmeau (FHP) cellular automation supplemented with the assumption of molecular chaos [13].

The main feature of LBM is the incorporation of the physics of microscopic processes, since it replaces the fluid by fraction particles according to a distribution function that considers the behaviour of a collection of particles a unit [14]. Consequently, LBM accurately captures the aerodynamics of high Reynolds number flows and pressure

fluctuations due to separated and reattached flows (main airframe noise source) and handles complex geometries without grids defined by complex analytical functions [15]. The program discretizes the Lattice-Boltzmann equation temporarily and spatially dividing the time into timesteps, in which each variable is calculated, and the computational domain into 3D-cells. At each timestep, the particles can either move in 18 directions to the neighboring cells, or stay in their position (0-vector) [15, 16].

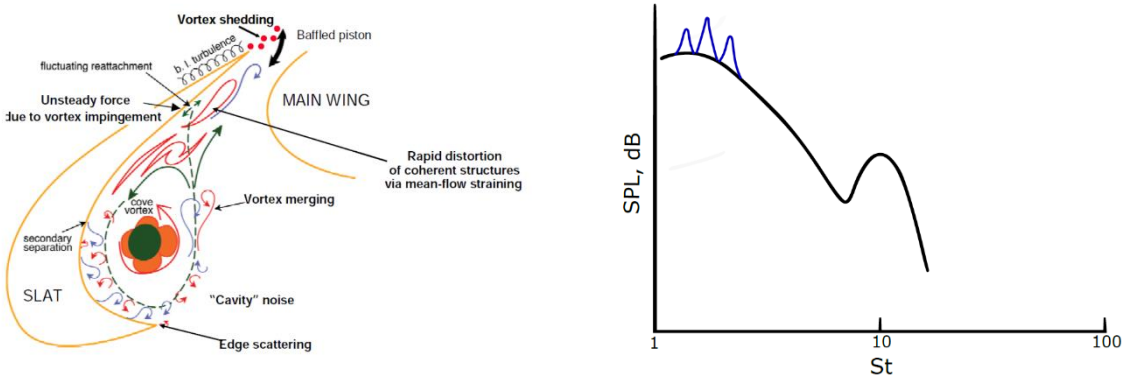

a) Flow around slat [8] *b) Typical slat spectrum [9]*

Figure 1: Slat noise characteristics

For the analysis of the far-field, PowerFLOW uses the FW-H acoustic analogy supplemented by the 1A formulation [17-20], which is included in the PowerACOUSTICS post-processing tool. Such an analogy propagates pressure fluctuations in the model surfaces in pressure fluctuations in the observer location, in this case, the microphone, assuming the aerodynamic noise as a quadrupole source.

2.1 Model

The model used for numerical studies was a three-element wing composed of a slat, a main wing element and a flap. Both flap and slat were fully extended and the angle of attack was 0^o. The model has 500 mm stowed chord and 250 mm span. Simulations were performed with the wing in an infinite configuration, for avoiding 3D effects on the wing tips.

2.1 Turbulence Model

PowerFLOW uses the κ-ε Re-Normalization Group (RNG) with extensions, which are equivalent to time-accurate Very Large Eddy Simulations (VLES) as a turbulence model. It also employs the eddy viscosity and Prandtl number to apply the effects of the unresolved (sub-grid) scale-flow properties to the resolved large scale and the universal law of the wall velocity profile coupled with the wall model pressure gradient to resolve the elements closest to the surface and determine the local skin friction.

2.2 Numerical Setup

The dimensions of the computational domain were 6500 mm x 1650 mm x 250 mm, where X and Z are in the streamwise and spanwise directions, respectively. The atmospheric conditions used in the simulations were P = 101325 Pa, T=300 K, $\rho = 1.177$ kg/m^3, and $\nu = 1.497 \times 10^{-5}$ m^2/s. The velocity inlet was set at 34 m/s, which correspond to 0.101 Mach number and 1.16×10^6 Reynolds number based on the stowed chord, and turbulence intensity at 0.21% with 1 mm turbulent scale. The outlet condition was set as no pressure gradient. The solid walls of the computational domain were set a free-slip

walls and the model walls were set as standard walls with an automatic transition model (the program calculates the transition).

The mesh on PowerFLOW is defined by refinement regions of different element sizes. Each region increases twice the size of the element of the previous region. The minimum element size was 0.17 times the thinnest slat trailing-edge thickness and the finest elements are located around the slat trailing-edge (for capturing the effect of the slat trailing-edge variations and vortex shedding). The element size in the FW-H measurement region was 0.25 mm, which is enough to capture the slat generation noise phenomena, according to Botero-Bolívar, L. et al., (2018) [21] and Pereira, L et al., (2018) [22]. The maximum element size was 128 mm, near the inlet and outlet walls, where the flow is almost constant. The outer region was modelled as a high viscosity fluid, or anechoic layer, for avoiding the reflection of waves approaching the computational domain. Such a condition is necessary for simulations since, otherwise, they would take long and their completion would not be viable.

The simulations were discretized into 103.23 x 10^6 elements and 4.9 x 10^6 timesteps, which correspond to 0.25 s in physical time, and took 22700 CPU hours.

2.3 Far-field Analysis

The surface pressure measurements for the FW-H analogy calculation were taken from a $3.5c_s$ x $4.7c_s$ x $2.4c_s$ (c_s is the slat chord) crop in the middle of the span (Figure 2) and propagated to a microphone at 0.835 m from the source. Measurements started at 0.147 s (for eliminating initial transient effects) at 82 kHz sampling frequency.

Power spectral values were normalized by the frequency for standardization and the reference value for the conversion to dB was 2 x 10^{-5} Pa. The time signal was segmented by the Hanning window and the band was a 100 Hz constant-width band, both for the calculation of the Fast Fourier Transformation (FFT).

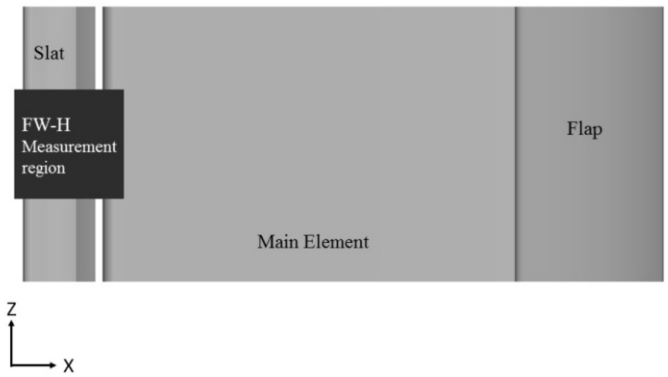

Figure 2: FW-H measurement region

2.4 Near-field Measurements

Fluid measurements were taken after the convergence of lift and drag coefficients. The time-average measurements of the fluid were taken at 71 Hz sampling frequency and instantaneous measurements were performed at 10 kHz sampling frequency. The latter were also used for the calculation of the Power Spectral Density (PSD) contours around the slat. The PSD was calculated under the same conditions of the far-field slat spectra.

3. RESULTS AND DISCUSSIONS

This chapter addresses aerodynamic and aeroacoustic results of simulations of three different slat Trailing-edge Thicknesses (TET), namely $0.0021c_s$, $0.0042c_s$, and $0.017c_s$. In each case, only the slat trailing-edge thickness was modified, whereas the

other geometry characteristics were kept constant. Steady aerodynamic results involve comparisons of lift and drag coefficients and pressure coefficient distribution. Unsteady aerodynamic results consist in the transient characteristics of the vortex shedding, and aeroacoustic results are the far-field spectra and PSD contours.

The slat trailing-edge thickness does not affect the wing performance significantly, since it influences neither the pressure coefficient distribution (Figure 3), nor the lift and drag coefficients. The major variations were 0.3% and 3% of lift and drag coefficients, respectively, between the thinnest and thickest slat trailing-edge configurations, of which the thickest one exhibited higher values.

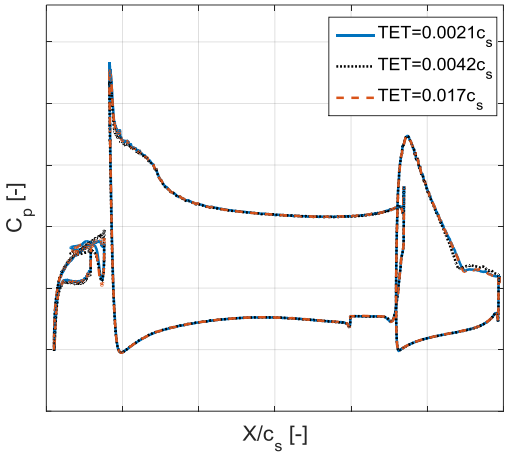

Figure 3: Pressure coefficient distribution

Figure 4 shows the results of the far-field spectra regarding Power Spectral Density (PSD) in function of Strouhal number (fU/c_s; U is the free stream velocity). The three cases exhibited the typical mid-frequency tones between 2 and 7 Strouhal number and also the high-frequency hump, whose frequency decreases as the trailing-edge thickness increases. Before and after the hump, the behaviour of the three spectra was the same and the Overall Sound Pressure Level (OSPL) was constant among the configurations.

Figure 5 displays the vortex shedding process behind the slat trailing-edge of the TET=0.0042c_s configuration (dt = 1.6 x 10^{-5} s). Two vortices are highlighted in the slat trailing-edge, i.e., one behind the upper side and the other from the lower side (which is more intense) with 180^o phase shift between them.

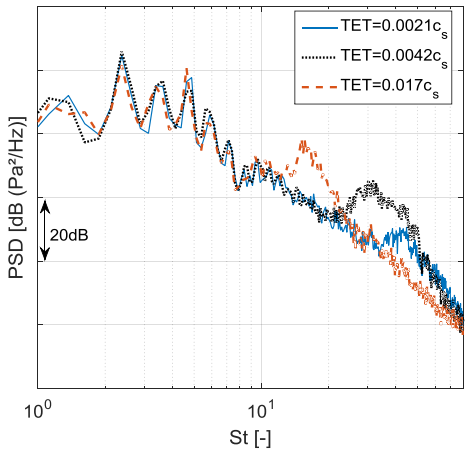

Figure 4: Far-field spectra

All configurations exhibited the vortex shedding behind the slat at different frequencies, which were consistent with those observed in the far-field. Table 1 (first column) displays the dominant Strouhal number observed in the far-field spectra and the second column shows the dimensional-less frequency (Strouhal number) calculated as the inverse of the period between two maximum pressure time derivatives in the same wake point.

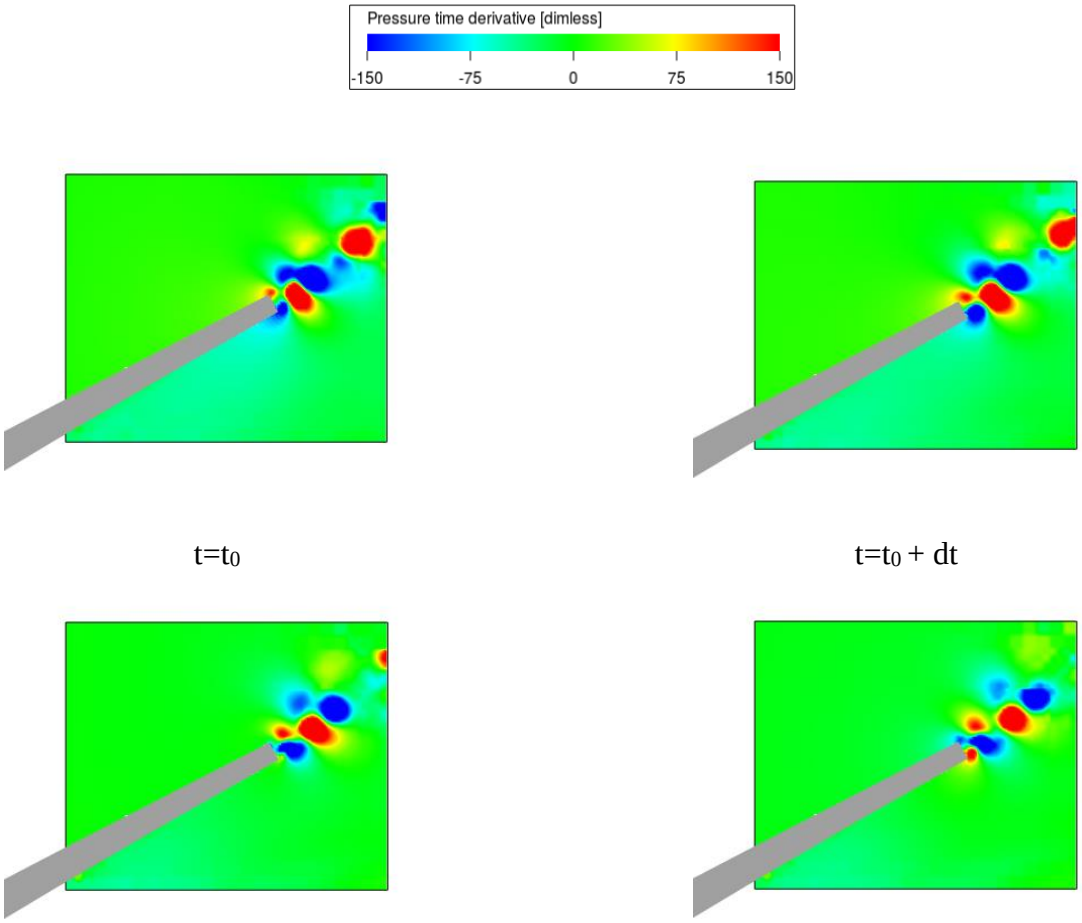

Figure 5: Pressure time derivative at the slat trailing-edge

Figure 6 shows the PSD in function of the Strouhal number calculated in the lower vortex core of all configurations. All cases exhibited a hump at high frequency, as reported in the literature [23]; however, the Strouhal number of the peak (table 1, column 3) is not consistent with that observed in the far-field spectra.

Table 1: Strouhal number of vortex shedding and slat spectra

Trailing-edge thickness	$St_{far\text{-}field}$	$St_{vortex\ shedding}$	$St_{vortex\ core\ spectrum}$
$0.0021c_s$	43.87	43	59.91
$0.0042c_s$	31.37	31.15	45.73
$0.0017c_s$	16.37	18.25	19.43

Bauer, A. B., (1961) [24] demonstrated the effective length for the calculation of the Strouhal number of a vortex shedding for a thin plate (similar to the slat trailing-edge) is $h=(d+2\delta^*)$, where d is the plate thickness - in this case, slat trailing-edge thickness-

and δ^* is the ideal Blasius boundary-layer displacement thickness. Therefore, the frequency of the hump in the far-field spectra and the boundary layer displacement thickness were used for the calculation of the characteristic Strouhal number of the vortex shedding (St=fU/δ*).

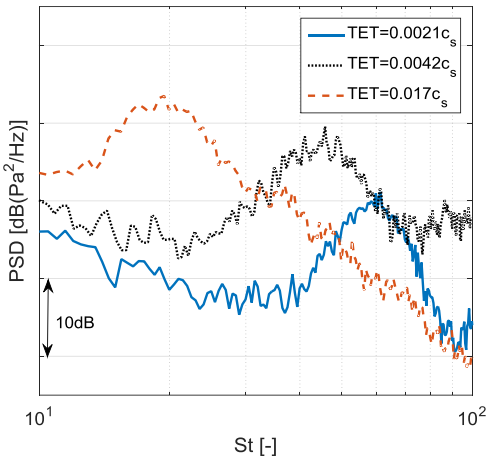

Figure 6: Power Spectral Density in the vortex core

Equation 1 obtained the boundary layer displacement thickness; the integration was made in the wake of the slat trailing-edge at $0.00074c_s$ behind it. Figure 7 displays the velocity profile at each configuration and its respective slat trailing-edge. The Strouhal number was close to 0.4 for all cases, which could be considered characteristic of all slat trailing-edge vortex shedding (see results in Table 2).

$$\delta^* = \int_{-x}^{x} 1 - \frac{u(x)}{U}$$

Equation 1 – Boundary layer displacement thickness

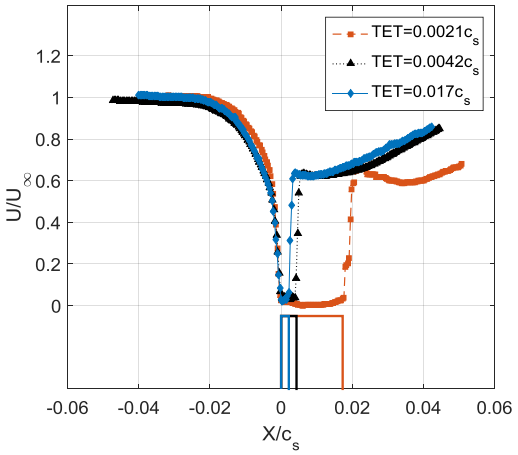

Figure 7: Velocity profile behind the slat trailing-edge

Imamura, T. et al., (2007) [12] also observed a relation between the high-frequency hump exhibited in the far-field and the dipole created in the trailing-edge calculating the PSD in the fluid around the slat trailing-edge at the same frequency of far-field hump (figure 8). Higher PSD levels were detected behind the tips of the slat trailing-edge (where the vortex shedding is located), which revealed the existence of a dipole of that specific frequency. On the other hand, Figure 9 shows the PSD at the far-field first tone frequency; higher levels of PSD are observed in the reattachment region. According

to the authors [12], higher pressure fluctuations at a low frequency around reattachment cause high-frequency fluctuations in the trailing-edge.

Table 2: Boundary layer displacement thickness and Strouhal number

Trailing-edge thickness	δ* [mm]	St
$0.0021c_s$	0.75	0.3875
$0.0042c_s$	1.08	0.4004
$0.0017c_s$	2.074	0.3996

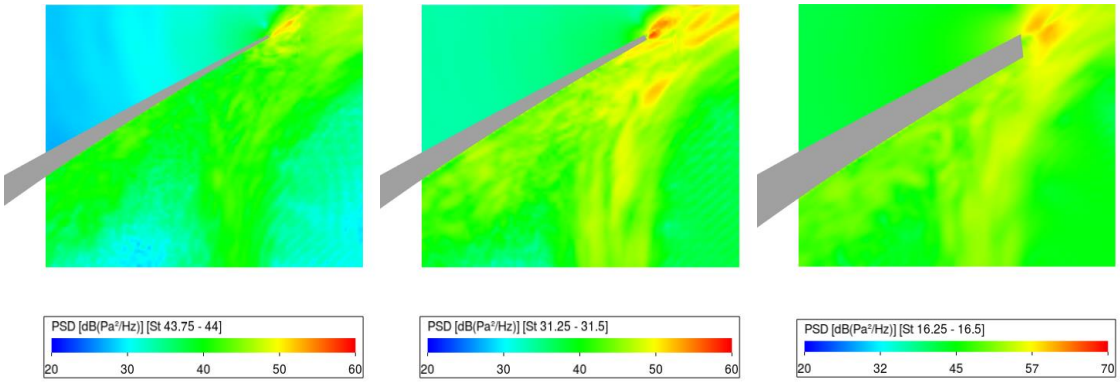

a) TET=0.0021c_s b) TET=0.0042c_s c) TET=0.017c_s

Figure 8: Power Spectral Density around slat trailing-edge

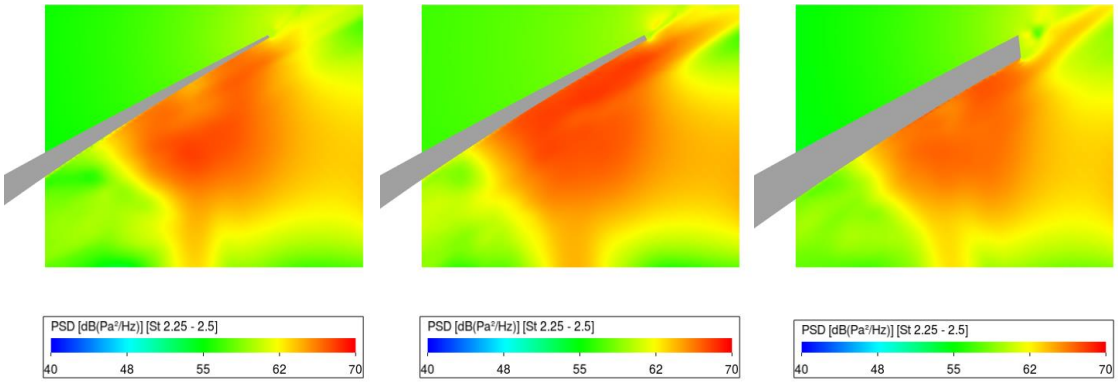

a) TET=0.0021c_s b) TET=0.0042c_s c) TET=0.017c_s

Figure 9: Power Spectral Density in the reattachment region

Figure 10 shows the PSD in function of Strouhal number of surface pressure fluctuations at the cusp, reattachment and trailing-edge at the mid-span of the three configurations. Although all configurations exhibited the same values in all frequency range, the hump at a high frequency at the cusp and trailing-edge is exhibited for the $0.0042c_s$ and $0.017c_s$ trailing-edge thickness configurations. The other configuration (TET=$0.0021c_s$) showed no high-frequency hump, since at that specific frequency the turbulence generates pressure fluctuations greater than those related to the vortex shedding.

4. CONCLUSIONS

Simulations of three different slat trailing-edge thicknesses of a 2D high-lift airfoil well captured spatially and temporally the vortex shedding in the slat wake in each case and the differences related to the differences in geometry. In the far-field spectrum, all

cases exhibited the same mid-frequency tones (same frequency and intensity values) and a high-frequency hump, whose frequency increases as the trailing-edge thickness decreases. The results showed such a hump is highly related to the vortex shedding behind the slat and its frequency is consistent with the vortex frequency, whereas the mid-frequency tones are associated with the interaction of the shear-layer and slat surface in the reattachment region.

Two vortices are formed in a blunt trailing edge with 180^0 phase difference and become a dipole of specific frequency in the far-field. Since the behaviour of the slat trailing-edge is similar to a thin plate, the characteristic Strouhal number for the hump is close to 0.4 if the characteristic length is the boundary layer displacement thickness for each case.

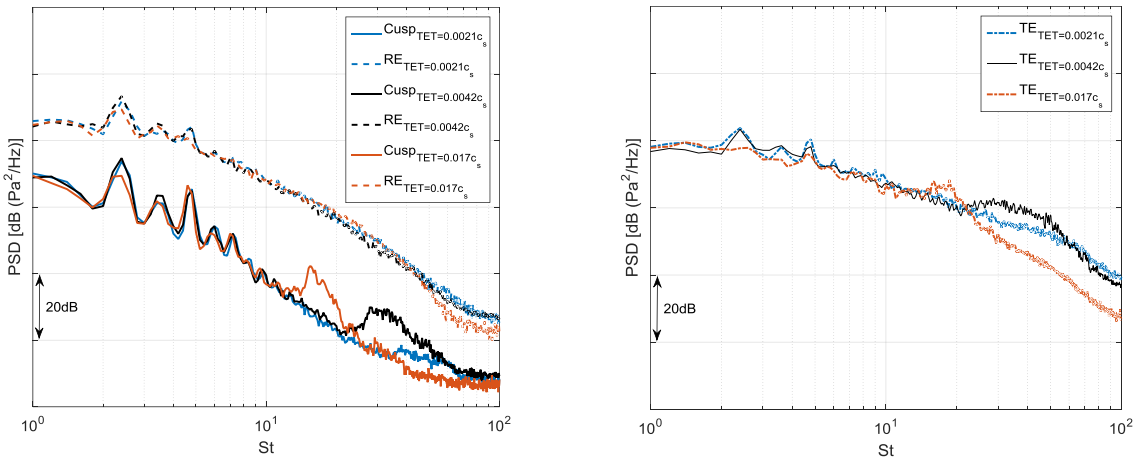

a) Cusp and reattachment *b) Trailing-edge*

Figure 10 – Power Spectral Density at surface point at midspan

5. ACKNOWLEDGEMENTS

The authors acknowledge the Conselho Nacional de Desenvolvimento Científico e Tecnológico (CNPq), Coordenação de Aperfeiçoamento de Pessoal de Nível Superior (CAPES) and A Financiadora de Estudos e Projetos (FINEP) for the financial support provided to this research.

6. REFERENCES

1. ICAO, I., "*Environmental report 2013*", Aviation and climate change, Vol. 2013.

2. Dobrzynski, W., Nagakura, K., Gehlhar, B., and Buschbaum, A., "*Airframe noise studies on wings with deployed high-lift devices*" 4th AIAA/CEAS Aeroacoustics Conference (1998)

3. Dobrzynski, W., "*Almost 40 Years of Airframe Noise Research – What did we achieve?*" Journal of Aircraft (2010)

4. Chow, L., Mau, K., and Remy, H., "*Landing gears and high lift devices airframe noise research*" 8th AIAA/CEAS Aeroacoustics Conference & Exhibit (2002)

5. Smith, M., Chow, L., and Molin, N., "*Attenuation of slat trailing-edge noise using slat gap acoustic liners*" 12th AIAA/CEAS Aeroacoustics Conference (27th AIAA Aeroacoustics Conference) (2006)

6. Airbus, "*Aircraft Noise - Technologies and Operations*" Tech. rep., Airbus (2007)

7. Pascioni, K. A., and Cattafesta, L.N., "*Aeroacoustic Measurements of Leading-Edge Slat Noise*" 22nd AIAA/CEAS Aeroacoustics Conference (2016)
8. Choudhari, M. M., and Khorrami, M. R., "*Slat Cove Unsteadiness Effect of 3D Flow Structures*" 44th AIAA Aerospace Sciences Meeting and Exhibit (2006).
9. Khorrami, M. R., Fares, E., Casalino, D. "*Towards full aircraft airframe noise prediction: lattice boltzmann simulations*" 20th AIAA/CEAS Aeroacoustics Conference, AIAA AVIATION Forum (2014).
10. Imamura, T., Ura, H., Yokokawa, Y., Enomoto, S., Yamamoto, K., and Hirai, T., "*Designing of slat cove filler as a noise reduction device for leading-edge slat*" 13th AIAA/CEAS (2007)
11. Dobrzynski, W., and Pott-Pollenske, M., "*Slat noise source studies for farfield noise prediction*" 7th AIAA/CEAS Aeroacoustics Conference and Exhibit (2001)
12. Imamura, T. et al. "*Simulation of the broadband noise from a slat using zonal les/rans hybrid method*" 45th AIAA Aerospace Sciences Meeting and Exhibit (2007)
13. Succi, S., Benzi, R., and Higuera, F., "*The lattice Boltzmann equation: A new tool for computational fluid-dynamics*" PhysicaD: Nonlinear Phenomena (1991)
14. Chen, S., and Doolen, G. D., "*Lattice Boltzmann method for fluid flows*" Annual review of fluid mechanics (1998)
15. Crouse, B., Freed, D., Balasubramanian, G., Senthooran, S., Lew, P.-T., and Mongeau, L., "*Fundamental aeroacoustic capabilities of the lattice-Boltzmann method*," Journal of Aircraft (2006)
16. He, X., Doolen, G. D., and Clark, T., "*Comparison of the lattice Boltzmann method and the artificial compressibility method for Navier–Stokes equations*" Journal of Computational Physics (2002)
17. Bres, G. A., Pérot, F., and Freed, D., "*A Ffowcs Williams-Hawkings solver for Lattice-Boltzmann based computational aeroacoustics*" Journal of Aircraft
18. Lighthill, M. J., "*On sound generated aerodynamically i. general theory*" In proceeding of Royal Society London A. London, United kingdom: The Royal Society (1952)
19. Farassat, F., "*Derivation of formulations 1 and 1a of farassat*" (2007)
20. Dowling, A. P., Williams, J. F. "*Sound and sources of sound*" (1983)
21. Botero-Bolívar, Laura et. al., "*Parametric Analysis of the Influence of Slat Geometry on Acoustic Noise*" 2018 AIAA/CEAS Aeroacoustics Conference (2018)
22. Pereira, Lourenco et. al., "*Experimental and Numerical Analysis of the Aerodynamic and Aeroacoustic Properties of a 2D High-LiftWing Model*" 2018 AIAA/CEAS Aeroacoustics Conference (2018)
23. Dhiraj, K and Kamal, P., "*Effect of tip vortices associated with a finite circular cylinder".* Hong Kong International Conference on Engineering and Applied Science (2015)
24. Bauer, A. B., "*Vortex shedding from thin flat plates parallel to the free stream".* Journal of the Aerospace Sciences (1961)